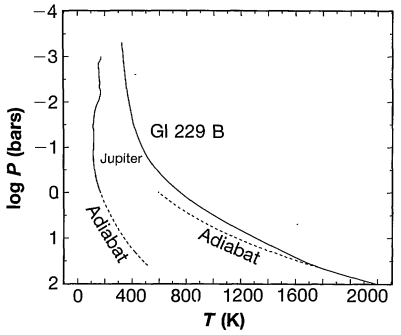

Fig. 4. Calculated atmospheric structure for Gl 229 B (solid curve); the dashed curve shows an adiabat corresponding to the deep interior temperature profile. For comparison, an observed profile for Jupiter (*16*) is shown (solid), along with its calculated prolongation into the adiabatic deep interior (dashed curve).

the temperature profile closely approaches an adiabatic profile at deeper levels because of efficient convection (Fig. 4). In some models, particularly the lower gravity models and those with $T_{eff} < 900$ K, the radiative-equilibrium lapse rate exceeds the adiabatic lapse rate over a several-bar region near $P = 1$ bar. These atmospheres exhibit two convective regions, a lower region presumably continuing to great depth and an upper, detached convective zone. Such a detached convective zone is also predicted for the atmosphere of Jupiter (*15*).

Our estimate of T_{eff} of 960 ± 70 K and a gravity between 800 and 2200 m s^{-2} for the brown dwarf Gl 229 B translates into masses and ages of 30 to 55 M_J and 1×10^9 to 5×10^9 years, respectively. As Eq. 1 and Fig. 3 indicate, gravity maps almost directly into mass, and ambiguity in the former results in uncertainty in the latter. Because the inferred mass of Gl 229 B exceeds that required for deuterium burning (*14*), deuterium-bearing molecules should not be present in its atmosphere. Although the near-infrared spectrum of Gl 229 B is dominated by H_2O, we confirmed the presence of CH_4 in the atmosphere from our modeling of its features at 1.6 to 1.8 μm, 2.2 to 2.4 μm, and 3.2 to 3.6 μm. In addition, we found a flux enhancement in the window at 4 to 5 μm throughout the T_{eff} range from 124 K (Jupiter) through 1300 K, and hence we believe that this band is a universal diagnostic for brown dwarfs and jovian planets.

REFERENCES AND NOTES

1. T. Nakajima *et al.*, *Nature* **378**, 463 (1995).
2. B. R. Oppenheimer, S. R. Kulkarni, K. Matthews, T. Nakajima, *Science* **270**, 1478 (1995).
3. K. Matthews, T. Nakajima, S. R. Kulkarni, B. R. Oppenheimer, in preparation; T. R. Geballe, S. R. Kulkarni, C. E. Woodward, G. C. Sloan, *Astrophys. J.*, in press.
4. A. Burrows, W. B. Hubbard, D. Saumon, J. I. Lunine, *Astrophys. J.* **406**, 158 (1993); J. I. Lunine, W. B. Hubbard, M. S. Marley, *ibid.* **310**, 238 (1986).
5. M. Mayor and D. Queloz, *Nature*, **378**, 355 (1995); G. W. Marcy and R. P. Butler, *Astrophys. J.*, in press; R. P. Butler and G. W. Marcy, *ibid.*, in press; G. Gatewood, *Bull. Am. Astron. Soc.* **28**, 885 (1996).
6. C. P. McKay, J. B. Pollack, R. Courtin, *Icarus* **80**, 23 (1989); M. S. Marley, C. P. McKay, J. B. Pollack, in preparation.
7. E. Anders and N. Grevesse, *Geochim. Cosmochim. Acta* **53**, 197 (1989).
8. The opacity calculations include collision-induced absorption by H_2–H_2 [A. Borysow and L. Frommhold, *Astrophys. J.* **348**, L41 (1990)] and H_2–He [C. Zheng and A. Borysow, *Icarus* **113**, 84 (1995), and references therein], free-free absorption by H_2^- [K. L. Bell, *J. Phys. B* **13**, 1859 (1980)], bound-free absorption by H^- [T. L. John, *Astron. Astrophys.* **193**, 189 (1988)], and Rayleigh scattering. We calculated the absorptions of NH_3, CH_4, and PH_3 using the HITRAN database [J. C. Hilico, M. Loete, L. R. Brown Jr., *J. Mol. Spectrosc.* **152**, 229 (1992)] with corrections and extensions. Additional tabulations [K. Strong, F. W. Taylor, S. B. Calcutt, J. J. Remedios, J. Ballard, *J. Quant. Spectrosc. Radiat. Transfer* **50**, 363 (1993)] were used where necessary for CH_4, especially shortward of 1.6 μm. Data for H_2O and H_2S were computed from a direct numerical diagonalization [R. B. Wattson and L. S. Rothman, *ibid.* **48**, 763 (1992)] by R. B. Wattson (personal communication). Absorption by CO [J. B. Pollack *et al.*, *Icarus* **103**, 1 (1993)] and PH_3 was included in the spectral models but not in the temperature profile computation. The baseline models assume that the atmosphere is free of clouds.
9. For the temperature profile computation, we treated the molecular opacity using the *k*-coefficient method [R. Goody, R. West, L. Chen, D. Crisp, *J. Quant. Spectrosc. Radiat. Transfer* **42**, 539 (1989)]. After a radiative-equilibrium temperature profile was found, we iteratively adjusted the atmosphere to self-consistently solve for the size of the convection zones, given the specified internal heat flux. Given the radiative-convective temperature-pressure profiles, we generated high-resolution synthetic spectra by solving the radiative transfer equation [P. Bergeron, F. Wesemael, G. Fontaine, *Astrophys. J.* **367**, 253 (1991)]. Eighteen thousand frequency points were used in the spectral region from 1 to 15.4 μm. These spectra were smoothed with a Gaussian-bandpass filter giving a final resolution of $\lambda/\Delta\lambda = 600$.
10. K. Matthews, T. Nakajima, S. Kulkarni, B. Oppenheimer, *Int. Astron. Union Circ. 6280* (1995).
11. B. Fegley Jr. and K. Lodders, *Icarus* **110**, 117 (1994).
12. K. Lodders, personal communication.
13. A. Burrows, D. Saumon, T. Guillot, W. B. Hubbard, J. I. Lunine, *Nature* **375**, 299 (1995).
14. D. Saumon *et al.*, *Astrophys. J.* **460**, 993 (1996).
15. T. Guillot, D. Gautier, G. Chabrier, B. Mosser, *Icarus* **112**, 337 (1994).
16. G. Lindal, *Astron. J.* **103**, 967 (1992).

17. D.S. is a Hubble Fellow. T.G. is supported by the European Space Agency. This research was supported by grants from NASA and NSF. We thank T. Geballe for digital versions of the Gl 229 B spectrum, K. Lodders for chemical-equilibrium calculations, and K. Zahnle for an insightful review.

21 March 1996; accepted 5 June 1996

Off-Resonance Conduction Through Atomic Wires

Ali Yazdani, D. M. Eigler, N. D. Lang

The electrical resistance of wires consisting of either a single xenon atom or two xenon atoms in series was measured and calculated on the basis of an atom-jellium model. Both the measurement and the calculation yielded a resistance of 10^5 ohms for the single–xenon atom system and 10^7 ohms for the two–xenon atom system. These resistances greatly exceeded the 12,900-ohm resistance of an ideal one-dimensional conduction channel because conduction through the xenon atoms occurs through the tail of the xenon 6*s* resonance, which lies far above the Fermi level. This conduction process in an atom-sized system can now be understood in terms of the electronic states of individual atoms.

Our understanding of the electron transport properties of macroscopic and mesoscopic bodies is relatively mature compared to our fledgling understanding of transport through nanometer-scale structures composed of just a few atoms. Transport through such structures is of particular interest because of its perceived importance in possible future device technologies. We address the question of how strong a role the electronic properties of a single atom play in determining the motion of electrons through a nanometer-sized object.

One might expect that the idealized view of one-dimensional (1D) transport, which predicts an electrical resistance quantized in units of $h/2e^2$ (where h is Planck's constant and e is the electron charge) of 12.9 kilohms, already captures most of the physics of electron transport down to the atomic scale (*1*). Research on mesoscopic conductors such as 2D electron gas devices realized in semiconductor heterostructures has shown the importance of such a conductance quantization in devices involving ballistic transport of electrons (*2*). However, conductance on a smaller scale, through a chain of just a few atoms, may depend on the atomic orbitals. More generally, one can ask if there are some principles by which we could understand the atomic-scale conduction process without extensive calculation in every case. We

A. Yazdani and D. M. Eigler, IBM Research Division, Almaden Research Center, 650 Harry Road, San Jose, CA 95120, USA.
N. D. Lang, IBM Research Division, Thomas J. Watson Research Center, Yorktown Heights, NY 10598, USA.

addressed these questions by performing atomically controlled measurements of the electrical transport through wires consisting of one or two Xe atoms with a scanning tunneling microscope (STM). Comparing the experimental results with fully self-consistent calculations of the resistance, we show that the resistance for such wires is mainly determined by the state-density contribution of the atomic resonances at the Fermi levels (E_F) of the electrodes, making the Xe wires a case of far-off resonance conduction.

Recent experiments with the STM and related devices (3) have shown that metallic point contacts, formed by bringing two metal surfaces together, show a residual jump-to-contact resistance of order 12 kilohms, the value expected for a 1D conductor with one ideal propagating channel of conduction. However, more recent measurements have shown that this resistance is in fact material-dependent, suggesting the importance of the atomic character in conduction through constrictions of atom-sized dimensions (3). Electrical conduction measurements through a single molecule of C_{60} have shown that the electronic structure of the molecule and its interaction with the electrodes plays a key role in determining its resistance (4). All such experiments suggest that we could learn much more about transport in small structures if we could perform measurements with knowledge of the specific number, location, and identity of the atoms in between two electrodes. We have used the STM's ability to manipulate individual Xe atoms to construct atomic wires and to measure the resistance for such wires. Furthermore, the experiments and calculations described here may serve as a test case to assess the ability of a general theoretical method recently described by Lang (5) in calculating the resistance of atomic wires. Our main goal is to investigate the sensitivity of the resistance in atom-sized wires to the number of atoms in the structure, their electronic structure, and their interaction with the macroscopic electrodes.

We measured the resistance of atomic wires consisting of one or two Xe atoms with a low-temperature (~5 K) STM operating in an ultrahigh vacuum. The Xe atomic wires are constructed between two macroscopic electrodes: the polycrystalline tungsten (W) tip of the STM and an atomically cleaned Ni(110) surface. Xenon atoms adsorbed on this surface at low temperature can be imaged (6) and repositioned (7) with a low-temperature STM. More importantly, the reproducible transfer of a Xe atom between the W tip and the Ni(110) surface (8) allowed us to prepare an atomically sharp STM tip with a Xe atom adsorbed at the very end of it.

Preferred binding of Xe atoms to low-coordination sites on a variety of different surfaces indicates that Xe binds to the outermost atom on the tip (8, 9). Further evidence for such binding comes from the enhanced imaging condition that occurs when we transfer a Xe atom from the surface to the tip (see Fig. 1A). Initially the Xe atom is on the surface and it appears as a bump 1.5 Å in height in the constant-current STM image (with junction impedance R_j = 20 megohms). We can transfer the Xe atom to the tip by applying a voltage pulse (≈+1.0 V) to the tip. Subsequent scanning (at R_j = 20 megohms) reveals the absence of the Xe at the surface, enhanced imaging resolution, and the retraction of the STM tip due to the increased current when the Xe is adsorbed on the tip.

After preparing the Xe-terminated tip, we measured the resistance of a single Xe atom coupled to two electrodes by recording the current I through the STM junction while moving the tip toward the surface. All of the measurements shown here were taken while the tip was biased at −10 mV relative to the sample (10, 11). We measured I for three different Xe-terminated tips, which were prepared in situ from the same polycrystalline W wire by allowing it to collide with the Ni surface or by using field emission from it such that there was a significant change in the microscopic configuration of its outermost atoms, and then terminating the tip with a Xe atom transferred from the surface. The data for the three Xe-terminated tips (Fig. 1B) indicate that, although there is some tip dependence in our experiment, the overall shape of the curve of I versus tip displacement D appears to be tip-independent and very different from that measured on the bare surface for the same tips, in the absence of the Xe. In particular, the Xe-terminated tips show strong deviation from exponential behavior in I as the tip approaches the sample, indicating the dominance of conduction through the Xe atom over conduction through tunneling of the electrons between the tip and the surface. In contrast, the "bare" tips show the expected exponential dependence of I on the width of the tunneling barrier over the same range of tip displacement. However, moving the "bare" metal tips closer to the surface results in a jump to contact and a discontinuity in I that is characteristic of a one-atom metallic contact (3) (Fig. 1B).

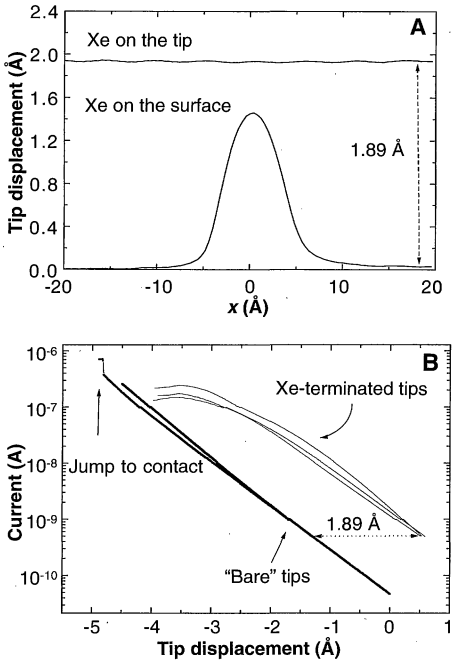

Fig. 1. (**A**) Two STM constant-current scans (at R_j = 20 megohms), one with the Xe on the surface and the other with the Xe on the tip. (**B**) Current measured through the STM junction (at a constant bias of −10 mV) as a function of tip displacement normal to the surface for both the "bare" and the Xe-terminated tips.

After each of the experiments with the Xe-terminated tips, we imaged the surface and found it to be undisturbed. We also confirmed the presence of the Xe atom as the outermost atom on the tip by transferring the Xe back to the surface and imaging it. The results in Fig. 1B for the Xe-terminated tips are offset from those for the "bare" tips by an amount equal to the difference in the initial height of the tip above the surface as demonstrated in Fig. 1A for one of the tips. When we made measurements with the Xe initially adsorbed on the surface, we obtained results similar to those plotted in Fig. 1B. Moreover, we found no detectable change in our results when the measurements were made at different locations within a unit cell of the Ni(110) surface.

Having measured the current through the STM junction with and without the Xe atom, we can extract the excess current due to the presence of the Xe atom by subtracting the I versus D curves in Fig. 1B. The results of this subtraction for the three different tips are shown in Fig. 2 as the corresponding resistance plotted as a function of the height of the tip above the surface. For Fig. 2, we used the procedure described in (12, 13) to determine the tip height above the surface. Also shown in Fig. 2 is the resistance of the "bare" metal-vacuum-metal junction that exhibits a jump to contact at $R \simeq 14$ kilohms. The Xe atom exhibits a greater resistance (by a factor of 7 or so) than that of a one-atom metal contact.

Our results dramatically changed when we measured the resistance of the STM junction with a chain of two Xe atoms in the junction instead of just one. We first

prepared a Xe-terminated tip and imaged the surface to locate another Xe atom on the surface. After centering the tip over the Xe atom on the surface, we measured the current through the junction as we moved the Xe-terminated tip toward the Xe adsorbed on the surface. The surface Xe atom was bound to the same surface site after the experiment as it was before; however, we cannot rule out lateral motion of the Xe atom during the experiment. Figure 2 shows that the resistance of the STM junction with a chain of two Xe atoms levels off near 10 megohms as the two Xe atoms approach one another (*12*). This resistance is 100 times that measured for the single Xe atom in close contact with both the tip and the surface.

To understand why the resistance of the Xe wire is so much greater than that for a one-atom metal link between two electrodes, we first consider the electronic structure of a Xe atom adsorbed on a metal electrode in a qualitative fashion. The Xe atom's state density at the E_F of the electrode comes almost entirely from the tail of a broadened 6*s* level, which is ~4 V above the E_F of the metal electrode (*6*). The electrical conduction through a Xe atom is dominated by the position and broadening of this far-off resonance. Calculations of tunneling conductance in a 3D resonant tunneling structure by Kalmeyer and Laughlin (*14*) indicate that the conductance of such structures is strongly dependent on the energy of the resonant state relative to E_F. On the basis of that model calculation, we believe that the greater resistance of the single Xe wire is based on the lack of strong overlap between the 6*s* level and states near E_F of the electrodes. Metal atoms adsorbed on metal electrodes have greater state density at E_F and hence exhibit lower resistance.

For a quantitative understanding of the conduction process in our Xe wires, we describe a detailed theoretical model and calculations. The computational procedure that we used with Xe atoms was used in (*5*) to determine the resistance of atomic wires consisting of one or more Al atoms, so here we only outline the method of calculation and report the results for the Xe wires. In this procedure, we represent the biased electrodes with the uniform-background (jellium) model (*15*) and compute the self-consistent electron density distribution for the system in the presence of one or two Xe atoms, whose cores are represented with the pseudopotential of Hamann, Schlüter, and Chiang (*16*). We calculated the wave functions for propagating states whose energies lie between the E_F values of the two electrodes, so that we could obtain the additional current that flows as a result of the presence of the Xe atom or atoms. Dividing the bias voltage by I, we obtained the resistance due to the presence of the Xe atom or atoms, which is directly comparable with the experimental results if the direct tunneling current between the tip and the sample is subtracted from the total I before the experimental value of the resistance (single-Xe case) is obtained or when the tunneling current is negligible compared to the total current (two-Xe case).

For a single Xe atom in the junction, we considered that the Xe is adsorbed onto one of the electrodes at a distance d and that it is a distance s from the other jellium-like electrode (model A, Fig. 3). We calculated the resistance in this case for a number of different s and d values (*17*). We plot the results in Fig. 3 as a function of $s + d$, which corresponds to the separation between the tip and the Ni surface. The experimental and theoretical resistances shown in Fig. 3 are comparable in value but different in their dependence on the separation. The experimental curves indicate a clear change of response when the Xe is close to both electrodes, whereas the theoretical curve appears nearly exponential over the entire range. In this regime, compression of the Xe atom by the tip may result in the lateral motion of the Xe atom out of the STM junction during the experiment. This possibility is not included in our model calculation and could account for the discrepancy. We also consider a more realistic model of the tip by including an extra metal adatom (W) in the junction (model B, Fig. 3). As demonstrated in Fig. 3 for two tip-surface separation values, this model falls somewhat closer to the experimental curve.

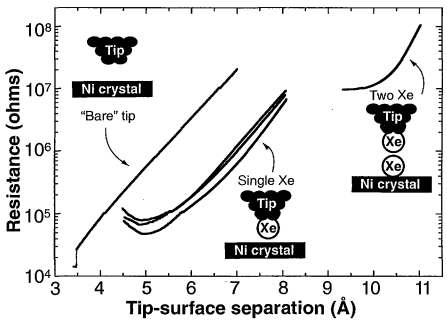

Fig. 2. The measured resistances due to one and two Xe atoms in the STM junction. For comparison, we have plotted the measured resistance of a "bare" STM junction. The data are shown as a function of tip-surface separation (*12*).

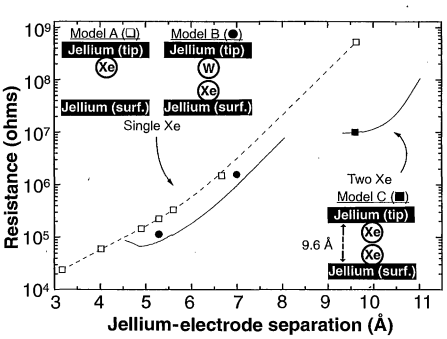

Fig. 3. Comparison of the various model calculations (symbols) and the experimental data (from Fig. 2, solid lines). We have shown only one of the data sets for the case of the single Xe as representative. Insets show the model geometries used for the calculations.

We then modeled the case of the atomic wire consisting of two Xe atoms in between the two jellium electrodes. We calculated the resistance for this wire with the two Xe atoms at their bulk separation (4.4 Å) and with each Xe atom bound to one of the electrodes at the theoretical binding distance (for an isolated Xe atom on a jellium surface) of 2.6 Å (*18*). In this case, the resistance was 9.4 megohms, in agreement with the experimental data (Fig. 3). The striking difference between the resistance of the two-Xe wire and that of the single-Xe case and the one-metal-atom contact, borne out by both the experiment and the calculation, can be understood by referring to the Landauer formula (*19*) for conductance of a single-channel conductor connected to two large contacts: $G = (2e^2/h)T$, where T is the transmission coefficient for the channel and the chemical potential difference for determining the conductance is that measured between points deep in the electrodes.

Now let us consider the transmission properties of two 1D potential wells in series (separated by barriers). If the wells are identical and we consider the conductance at the resonant energy of the well, we expect T to be equal to unity whether we have one or two wells. This situation represents the case of metal atoms with wide resonances centered near the E_F values for the two electrodes (*5*), where we expect the resistance to be of the order of 12 kilohms and to be insensitive to the number of atoms in the junction. The case of Xe, however, involves far-off resonance conduction where T is very small; the T_s for the series of wells, that is, a chain of Xe atoms, can be quite different from that for one well. For example, in our 1D analogy we expect T_2 of the double-well case to be $\sim T_1^2/4$ (*20*). Given this relation, it is not surprising that the resistance of the two–Xe atom wire is 100 times that for a single–Xe atom wire.

Note added in proof. Earlier computations for the single-Xe case were carried out as part of the work reported by Eigler *et al.* (*6*) and also by Joachim *et al.* (*21*).

REFERENCES AND NOTES

1. C. W. J. Beenaker and H. van Houten, *Solid State Phys.* **44**, 1 (1991), and references therein.
2. B. J. van Wees *et al.*, *Phys. Rev. Lett.* **60**, 848 (1988).

3. L. Olesen *et al.*, *ibid.* **72**, 2251 (1994); J. M. Krans and J. M. van Ruitenbeek, *Phys. Rev.* **50**, 17659 (1994); J. M. Krans *et al.*, *Nature* **375**, 767 (1995), and references therein.
4. C. Joachim, J. K. Gimzewski, R. R. Schlittler, C. Chavy, *Phys. Rev. Lett.* **74**, 2102 (1995).
5. N. D. Lang, *Phys. Rev. B* **52**, 5335 (1995).
6. D. M. Eigler, P. S. Weiss, E. K. Schweizer, N. D. Lang, *Phys. Rev. Lett.* **66**, 1189 (1991).
7. D. M. Eigler and E. K. Schweizer, *Nature* **344**, 524 (1990).
8. D. M. Eigler, C. P. Lutz, W. E. Rudge, *ibid.* **352**, 600 (1991).
9. D. M. Eigler and C. P. Lutz, unpublished results.
10. We measured *I* versus *V* and *dI/dV* versus *V*; both measurements indicated that, to within 5%, there was no *V* dependence over the range ±30 mV to the resistances we report here.
11. We have held the voltage drop across the STM junction constant as we extended the *z*-piezo toward the surface. Adjustments in the applied voltage become important when the resistance of the junction becomes comparable to the finite input resistance (20 kilohms) of our electrometer.
12. To determine tip-surface separation, we have compared the measured *I* versus *D* curves for the "bare" tips to a calculation by Lang (*13*), which models the STM junction as two jellium surfaces with a single atom adsorbed on one of the surfaces. This calculation shows that an impedance of 2×10^7 ohms for an STM junction corresponds to a tip height above the surface of ~7 Å. We have found Lang's calculation to be consistent with *I* versus *D* measurements taken on this same Ni surface (*6*). We used this calibration, together with the measured changes in tip height due to the presence of one or two Xe atoms in the junction, to determine the tip-surface separation.
13. N. D. Lang, *Phys. Rev. Lett.* **36**, 8173 (1987); J. K. Gimzewski and R. Möller, *Phys. Rev. B* **36**, 1284 (1987).
14. V. Kalmeyer and R. B. Laughlin, *Phys. Rev. B* **35**, 9805 (1987).
15. N. D. Lang, *Solid State Phys.* **28**, 225 (1973).
16. D. R. Hamann, M. Schlüter, C. Chiang, *Phys. Rev. Lett.* **43**, 1494 (1979); G. B. Bachelet, D. R. Hamann, M. Schlüter, *Phys. Rev. B* **26**, 4199 (1982).
17. We set $d = 2.6$ Å, the equilibrium Xe binding distance (*18*), except when $s < 2.6$ Å where we then set $s = d$ to account for the compression of the Xe atom.
18. N. D. Lang, *Phys. Rev. Lett.* **46**, 842 (1981).
19. See, for example, R. Landauer, *Phys. Scr.* **T42**, 110 (1992); *J. Phys. Condens. Matter* **1**, 8099 (1989); Y. Imry, in *Directions in Condensed Matter Physics: Memorial Volume in Honor of Shang-keng Ma*, G. Grinstein and G. Mazenko, Eds. (World Scientific, Singapore, 1986), pp. 101–163.
20. M. Büttiker, *IBM J. Res. Dev.* **32**, 63 (1988); E. O. Kane, in *Tunneling Phenomena in Solids*, E. Burstein and S. Lundqvist, Eds. (Plenum, New York, 1969), pp. 1–11.
21. C. Joachim *et al.*, *Europhys. Lett.* **20**, 697 (1992).
22. We thank D. J. Auerbach, R. Landauer, C. P. Lutz, and C. T. Rettner for helpful discussions. We are also indebted to C. P. Lutz for technical assistance.

12 February 1996; accepted 29 April 1996

Shape-Controlled Synthesis of Colloidal Platinum Nanoparticles

Temer S. Ahmadi, Zhong L. Wang, Travis C. Green, Arnim Henglein, Mostafa A. El-Sayed*

The shapes and sizes of platinum nanoparticles were controlled by changes in the ratio of the concentration of the capping polymer material to the concentration of the platinum cations used in the reductive synthesis of colloidal particles in solution at room temperature. Tetrahedral, cubic, irregular-prismatic, icosahedral, and cubo-octahedral particle shapes were observed, whose distribution was dependent on the concentration ratio of the capping polymer material to the platinum cation. Controlling the shape of platinum nanoparticles is potentially important in the field of catalysis.

Colloidal metal particles are of interest because of their use as catalysts (*1*), photocatalysts (*2*), adsorbents and sensors (*3*), and ferrofluids (*4*) and because of their applications in optical (*5*), electronic (*5*), and magnetic devices (*3*). Catalytic reactivity depends on the size and the shape of the nanoparticles, and therefore the synthesis of well-controlled shapes and sizes of colloidal particles could be critical for these applications.

Many studies on colloidal particles have focused on the control of particle sizes and their growth kinetics and have related particle size and catalytic activity (*6*). Moreover, research has shown that the degree of polymerization (*1*) and the concentration of the stabilizing polymer (*2*, *7*) influence the size distribution, stability, and catalytic activity of colloidal particles. For example, a recent study (*7*) has shown that a higher ratio of capping material to metal produces smaller Au particles. However, shape control has been much more difficult to achieve, and the influence of particle shape on catalytic activity has not been reported to date.

The morphology of colloidal Au has been studied (*8*, *9*), and shape-controlled synthesis of Au particles forming platelike trigons has been explained (*10*) in terms of the Kossel-Stranski theory of face-selective growth of crystals. Shape-controlled synthesis of polymer-protected Cu particles exhibiting platelike hexagonal morphology has also been reported (*11*). Recently, the morphologies of Pt colloidal particles were studied by means of ultraviolet-visible spectrophotometry and transmission electron microscopy (TEM) (*12*). A parameter *S*, derived from the optical spectrum, has been suggested as a measure of particulate shape and the degree of dispersion (*12*).

In this report, we describe a method for the synthesis of colloidal Pt nanoparticles with controlled shapes. By changing the ratio of the concentration of the capping material to that of Pt^{2+} at room temperature, we were able to change the distribution of Pt nanoparticle shapes.

The Pt nanoparticles were prepared by the method of Rampino and Nord (*13*) and Henglein *et al.* (*14*). A solution of 1×10^{-4} M K_2PtCl_4 was prepared in 250 ml of water, to which we added 0.2 ml of 0.1 M sodium polyacrylate (sample 1). We then bubbled Ar gas through the solution for 20 min. We then reduced the Pt ions by bubbling H_2 gas at a high flow rate through the solution for 5 min. The reaction vessel was then sealed, and the solution was left overnight. After 12 hours, the solution turned lightly golden and the absorption spectrum showed the formation of colloidal Pt. We prepared samples 2 and 3 by adding to the starting solution 1.0 and 0.5 ml of the 0.1 M polyacrylate solution, respectively, and following the same procedure. The initial ratios of the concentration of the capping material to that of the metal cation in the solution were therefore 1:1, 5:1, and 2.5:1 in samples 1, 2, and 3, respectively.

Because the concentration of the capping polymer was changed in the preparation of samples 1 through 3, the pH values of the starting solutions were also different. The variation of pH in the three solutions was small; it changed from 7.5 to 7.65 when the concentration of the polymer was changed by a factor of 5 (going from sample 1 to sample 2). In our synthesis, we adjusted the initial pH of the solutions to 7.5 in all three solutions.

We investigated the structures of the Pt particles using a Hitachi HF-2000 field emission gun TEM (200 kV) with a point-to-point image resolution of better than 0.23 nm and a lattice resolution of 0.1 nm. We recorded the experimental images digitally using a charge-coupled device camera, which allows subsequent processing and quantitative modeling. We prepared the

T. S. Ahmadi, T. C. Green, M. A. El-Sayed, School of Chemistry and Biochemistry, Georgia Institute of Technology, Atlanta, GA 30332, USA.
Z. L. Wang, School of Material Sciences and Engineering, Georgia Institute of Technology, Atlanta, GA 30332, USA.
A. Henglein, Hahn-Meitner Institut, Abteilung Kleinteilchenforschung, 14109 Berlin, Germany.
*To whom correspondence should be addressed.